Journal of Hydrology 556 (2018) 901–912

Contents lists available at ScienceDirect

Journal of Hydrology

journal homepage: www.elsevier.com/locate/jhydrol

Addressing the mischaracterization of extreme rainfall in regional climate model simulations – A synoptic pattern based bias correction approach

Jingwan Li [a], Ashish Sharma [a,*], Jason Evans [b], Fiona Johnson [a]

[a] School of Civil and Environmental Engineering, University of New South Wales, Sydney, New South Wales 2052, Australia
[b] Climate Change Research Centre and ARC Centre of Excellence for Climate System Science, School of Biological, Environmental and Earth Sciences, University of New South Wales, Sydney, New South Wales, Australia

ARTICLE INFO

Article history:
Available online 18 May 2016

Keywords:
Bias correction
Extreme rainfall
Synoptic patterns
Climate change
Self-organizing maps classification
Regional climate models

SUMMARY

Addressing systematic biases in regional climate model simulations of extreme rainfall is a necessary first step before assessing changes in future rainfall extremes. Commonly used bias correction methods are designed to match statistics of the overall simulated rainfall with observations. This assumes that change in the mix of different types of extreme rainfall events (i.e. convective and non-convective) in a warmer climate is of little relevance in the estimation of overall change, an assumption that is not supported by empirical or physical evidence. This study proposes an alternative approach to account for the potential change of alternate rainfall types, characterized here by synoptic weather patterns (SPs) using self-organizing maps classification. The objective of this study is to evaluate the added influence of SPs on the bias correction, which is achieved by comparing the corrected distribution of future extreme rainfall with that using conventional quantile mapping. A comprehensive synthetic experiment is first defined to investigate the conditions under which the additional information of SPs makes a significant difference to the bias correction. Using over 600,000 synthetic cases, statistically significant differences are found to be present in 46% cases. This is followed by a case study over the Sydney region using a high-resolution run of the Weather Research and Forecasting (WRF) regional climate model, which indicates a small change in the proportions of the SPs and a statistically significant change in the extreme rainfall over the region, although the differences between the changes obtained from the two bias correction methods are not statistically significant.

1. Introduction

The impact of climate change is one of the major challenges in water supply and flood risk management. Both observations and model simulations indicate a general increasing trend in the rainfall intensity and variability on a global scale (Alexander et al., 2006; BoroumandJazi et al., 2012; Singleton and Toumi, 2013). This has significant implications on the estimation of design flood for future climates (Ishak et al., 2013) which is estimated through projections of future rainfall and its distribution in time (Wasko and Sharma, 2015) and space (Li et al., 2015).

While the impact of climate change on the hydrological cycles over the historical period can be analyzed from observations and climate model simulations, the effects of future changes can only be studied using climate model projections. Global circulation models (GCMs) are often used in climate impact studies. However, GCMs are usually unable to resolve small spatial and temporal scales that are relevant to hydrological processes. To refine the outputs from a coarse GCM simulation to the fine scale, statistical or dynamical downscaling approaches are employed. While statistical downscaling uses selected atmospheric predictor variables to derive the downscaled rainfall, dynamical downscaling resolves physical processes at the local scale by using regional climate models (RCMs) nested within GCM outputs or reanalysis datasets. As such, RCMs were found capable of reproducing important mesoscale patterns of observed precipitation and reflect the topographic effects on precipitation (Frei et al., 2006). In addition, RCMs, mostly run at 10–50 km horizontal resolution, were generally found better in representing daily precipitation extremes than their parent GCMs, and some studies also show that RCMs can better represent subdaily precipitation extremes (Westra et al., 2014).

* Corresponding author.
E-mail address: a.sharma@unsw.edu.au (A. Sharma).

http://dx.doi.org/10.1016/j.jhydrol.2016.04.070
0022-1694/

Although RCMs show promise in their ability to model rainfall extremes, there remain some concerns. Since most RCMs are available at a spatial resolution of 10 km or coarser, a convection parameterization scheme is required to address the convective effect that cannot be resolved on a coarse grid. Significant uncertainties remain in convective parametrization schemes and hence in the rainfall they simulate. Modeling at convection permitting resolutions (below 4 km) allows the removal of the convection scheme and its associated uncertainties (Olsson et al., 2014). Regardless, other model uncertainties lead to biases in the rainfall output, which have to be corrected before any climate impact studies. A range of bias correction techniques have been developed and most of them deal with the total precipitation on daily or monthly time scales (Bordoy and Burlando, 2012; Grillakis et al., 2013; Gutjahr and Heinemann, 2013; Johnson and Sharma, 2012; Lafon et al., 2013; Piani et al., 2010; Raneesh and Thampi, 2013), with only recent work attempting to bias correct convection-permitting resolution simulations (Argüeso et al., 2013). A review of the strengths and weaknesses of some commonly used bias correction methods for total precipitation is presented in Sachindra et al. (2014). These bias correction methods can be essential divided into three groups: (1) monthly bias correction (MBC), (2) nested bias correction (NBC) and (3) quantile mapping. The MBC and NBC approaches only correct the statistics of the climate variables, whereas the quantile mapping corrects the entire distribution of the variable (Nguyen et al., 2016). Hence, the quantile mapping is considered more effective in correcting the daily precipitation time series. While most studies target on correcting the total daily (or monthly) precipitation, only a few of them focus on extreme rainfall in the bias correction (Friederichs, 2010; Sunyer et al., 2015; Wong et al., 2014), resulting in the bias corrected extremes often systematically under- or over-representing observed extremes for current climate simulations.

While the accurate representation of sub-grid processes in RCMs remains a challenge, they are quite robust regarding simulating large-scale atmospheric circulations. Bárdossy and Pegram (2011) applied bias correction on daily precipitation corresponding to circulation patterns (CPs) derived from sea level pressure (SLP) fields and compared the results with those obtained from a quantile mapping bias correction on the overall distribution of daily precipitation. They found that the circulation based bias correction method produced different results to the universal method. The extent of this difference was proportional to the difference of the CP-dependent precipitation between model simulations and observations. Two main questions arise from their study that are worthy of further consideration. The first is that Bárdossy and Pegram (2011) did not incorporate in their methodology the biases and changes in the frequency of occurrence of each CP. Recent studies have suggested that a warming climate can cause changes in the occurrence of certain circulation patterns. For example, Horton et al. (2015) found that the occurrence of anticyclonic circulation patterns was increasing, while the occurrence of cyclonic circulation patterns was decreasing in summer over parts of Europe by using the daily 500 hPa geopotential height anomaly from NCAR/NCEP-R1 over the period of 1970–2013. Secondly the focus of Bárdossy and Pegram's (2011) was on daily rainfall totals, but as discussed above, trends in and future projections for rainfall extremes can differ quite substantially from the behavior of daily rainfall totals.

In this study, we propose an alternative bias correction method for rainfall extremes by focusing on the ability of RCMs to represent extremes through specified synoptic patterns (SPs). In formulating the approach, systematic biases in the frequency of the SPs associated with the extremes, are addressed, along with the bias in the distribution of rainfall associated with each SP considered. The next section summarizes the data used in this study. Section 3 describes the methodology including a detailed discussion of the method used to identify the synoptic patterns as well as the bias correction method used. Section 4 presents the results obtained from using the synoptic pattern based method and the quantile mapping approach. Section 5 discusses the limitation of the proposed method followed by our conclusions in Section 6.

2. Observations and RCM Data

The rainfall extremes simulated by the RCM was bias corrected based on the assumption that the statistics of bias for the current climate apply to the future climate. As potential changes in the synoptic circulation patterns could alter the intensity and frequency of the extreme rainfall, the bias correction was conditioned on the identified synoptic circulation patterns. As such, the rainfall and synoptic pattern data from both observations and model simulations are used in this study.

2.1. Observed data

The observed rainfall data used in this work is from the Australian Bureau of Meteorology. Daily rainfall data from 204 rainfall gauges (black dots on Fig. 1a) that cover the entire period of 1990–2009 are used to extract the 1-day and 3-day annual maximum rainfall. Daily rainfall is recorded each day at 9 am local time, measuring the accumulated rainfall during the previous 24 h.

The observed synoptic weather data are obtained from the National Center for Environmental Prediction/National Center for Atmospheric Research (NCEP/NCAR) Reanalysis Project (Gudmundsson et al., 2012), referred as NNRP in the rest of the paper. Daily sea level pressure extracted from the $2.5^\circ \times 2.5^\circ$ (equivalent to 210 km) resolution grids of NNRP is used for the synoptic pattern classifications over southeast Australia with each grid cell indicated by the red asterisks on Fig. 1b. As the reanalysis is produced via a data assimilation scheme, which injects contemporaneously observed data every 6–12 h into the numerical weather prediction model to correct the errors (Carton and Giese, 2008), it is considered to be representative of observations. As the study region is dominantly affected by the westerly winds, the domain of the synoptic patterns mainly focuses on the west of the study region.

2.2. RCM data

The simulated rainfall extremes are obtained from an RCM running at a 2-km horizontal resolution over the Sydney region. This 2-km resolution domain is double nested within 10-km and 50-km resolution domains. The simulations at these lower resolutions have been evaluated across a range of timescales (Evans and McCabe, 2010, 2013; Evans and Westra, 2012) and was found to perform well. This 2-km resolution RCM was developed using the Weather Research and Forecasting (WRF) model system (Chandra et al., 2015) and used the following physics schemes: Thompson microphysics scheme (Thompson et al., 2004); the Rapid Radiative Transfer Model (RRTM) longwave radiation scheme; the Dudhia shortwave radiation scheme; Monin–Obukhov surface layer similarity theory; Noah land-surface model (LSM); and the Yonsei University planetary boundary layer (PBL) (Argüeso et al., 2014). This RCM covers the historical period of 1990–2009 and the future period of 2040–2059. There are two different runs for the historical period: one with boundary conditions from NNRP, and the other having its boundary conditions from CSIRO Mk3.5 outputs. For the future period, only one run is available and is forced by the outputs of CSIRO Mk3.5 under the SRES A2 emission scenario. The use of the 2 km resolution RCM ensures that precipitation extremes

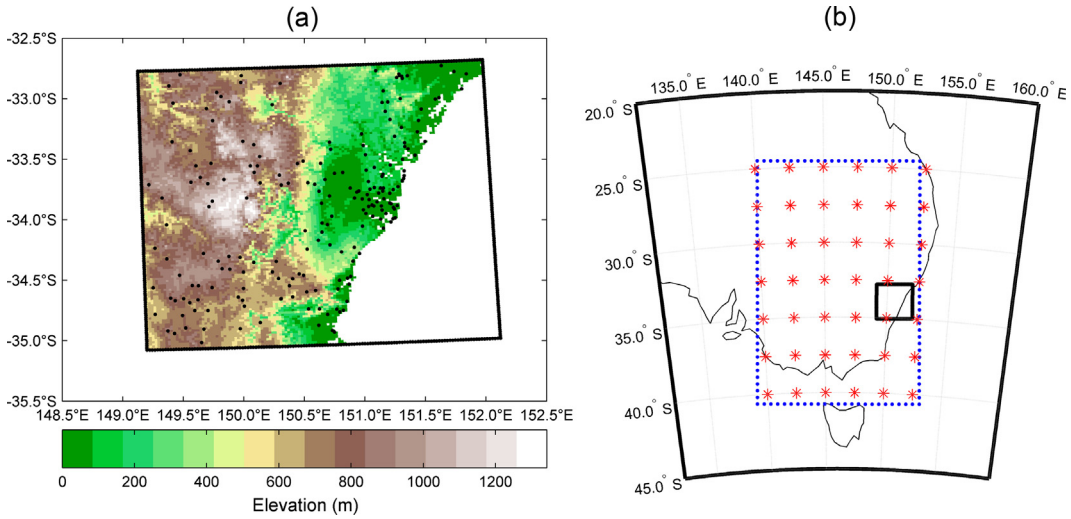

Fig. 1. The spatial domain used for the SPBC approach. (a) Topography on the 2-km RCM domain with 204 rainfall stations indicated by black dots. (b) Synoptic pattern field on 50-km RCM domain (delineated by the blue dots) with NNRP reanalysis data points marked by red asterisks. (For interpretation of the references to color in this figure legend, the reader is referred to the web version of this article.)

Table 1
Averaged statistics of the daily rainfall at 197 gauged sites estimated for both observations and RCM simulations.

	Mean (mm)	Standard deviation (mm)	PDF overlapping coefficient
Obs.	8.67	13.59	N/A
WRF/NNRP	7.52	15.31	0.82
WRF/MK3.5	11.00	25.47	0.74

related to convection are produced explicitly within the model and are not dependent on the choice of convection parameterization.

Table 1 shows some of the averaged statistics calculated using the daily rainfall data at the 197 gauged sites. The WRF/NNRP simulated the daily rainfall close to the observations with the mean and standard deviation only slightly higher than the observations. The PDF overlapping coefficient, which was estimated as the common area under the two probability density function (PDF) curves (Clemons and Bradley, 2000) representing the daily rainfall from the observations and RCM simulation, for WRF/NNRP is 0.82. This suggests that the WRF/NNRP captured the daily rainfall distribution reasonably well. Compared with WRF/NNRP, WRF/MK3.5 moderately overestimated the mean of daily rainfall, and the daily rainfall distribution shares less common area with the observations.

The simulated synoptic weather data are from the 50-km RCM that covers a large area of southeast Australia, which encompasses the 2-km RCM domain as shown in Fig. 1b. Eight grids along the boundaries of the original domain of the 2-km and 50-km RCMs are excluded in this study to avoid the boundary transition effect. Fig. 1 shows the domain used from each RCM for the analysis. The reason for choosing a larger domain for synoptic data is to capture the synoptic scale (>1000 km) weather patterns that are responsible for the extreme rainfall. It should be noted that the 50 km domain is off-center to the 2 km domain as the study region is dominated by westerly winds. It should also be noted that both RCMs (50-km and 2-km resolution) use similar boundary conditions and physical schemes, hence the circulation patterns simulated by the 50-km resolution RCM are directly linked to the extreme rainfall simulated by the 2-km resolution RCM.

3. Methodology

Existing bias correction methods usually correct the future projections without considering the possible change of the composition of the types of rainfall extremes. Fig. 2a illustrates one of the commonly used bias correction approaches, quantile mapping, which implicitly assumes the biases for all types of rainfall extremes are the same. However, it is possible that the biases vary with the types of extreme rainfall. In addition, the proportion of each extreme rainfall type may change as a result of climate change. As for the number of extreme rainfall types, defined by the number of SPs, RCM simulations may also differ from observations. A systematic change in the mix of extreme rainfall event types is also supported by the increase in observed convection driven rainfall extremes around the world (Berg et al., 2013).

In this study, we propose a new approach to correct biases of rainfall extremes simulated by the RCM for the future climate using the relationship between the large-scale synoptic weather patterns and the rainfall extremes defined as annual maxima. The days with rainfall extremes are first divided into n distinctive clusters based on the classification of synoptic weather patterns. Fig. 2b gives an illustration of this method. Here only 2 clusters are used for simplicity of presentation. As shown in the left panels of Fig. 2b, the bias behavior varies with different clusters (represented by the different colors), and, therefore, the correction for different clusters will be different. Once the distribution of each type of the rainfall extremes is corrected, the proportion of each type is also corrected as illustrated by the color bars at the bottom of Fig. 2b. Finally, the weighted combination of the different types is estimated to form a distribution representing overall rainfall extremes.

The proposed method does add a certain complexity to the conventional quantile mapping approach. To decide whether it is worth implementing the SP based method, the add-on value of using SPs will be evaluated by comparing the corrected distribution for future extreme rainfall using the synoptic pattern based bias correction (SPBC) approach with that using the quantile mapping method. The Kolmogorov–Smirnov (KS) test is employed to test the significance of this add-on value. If the test returns a non-significant decision, then it is not necessary to apply the proposed method as it will produce statistically indistinguishable results as the simple quantile mapping method.

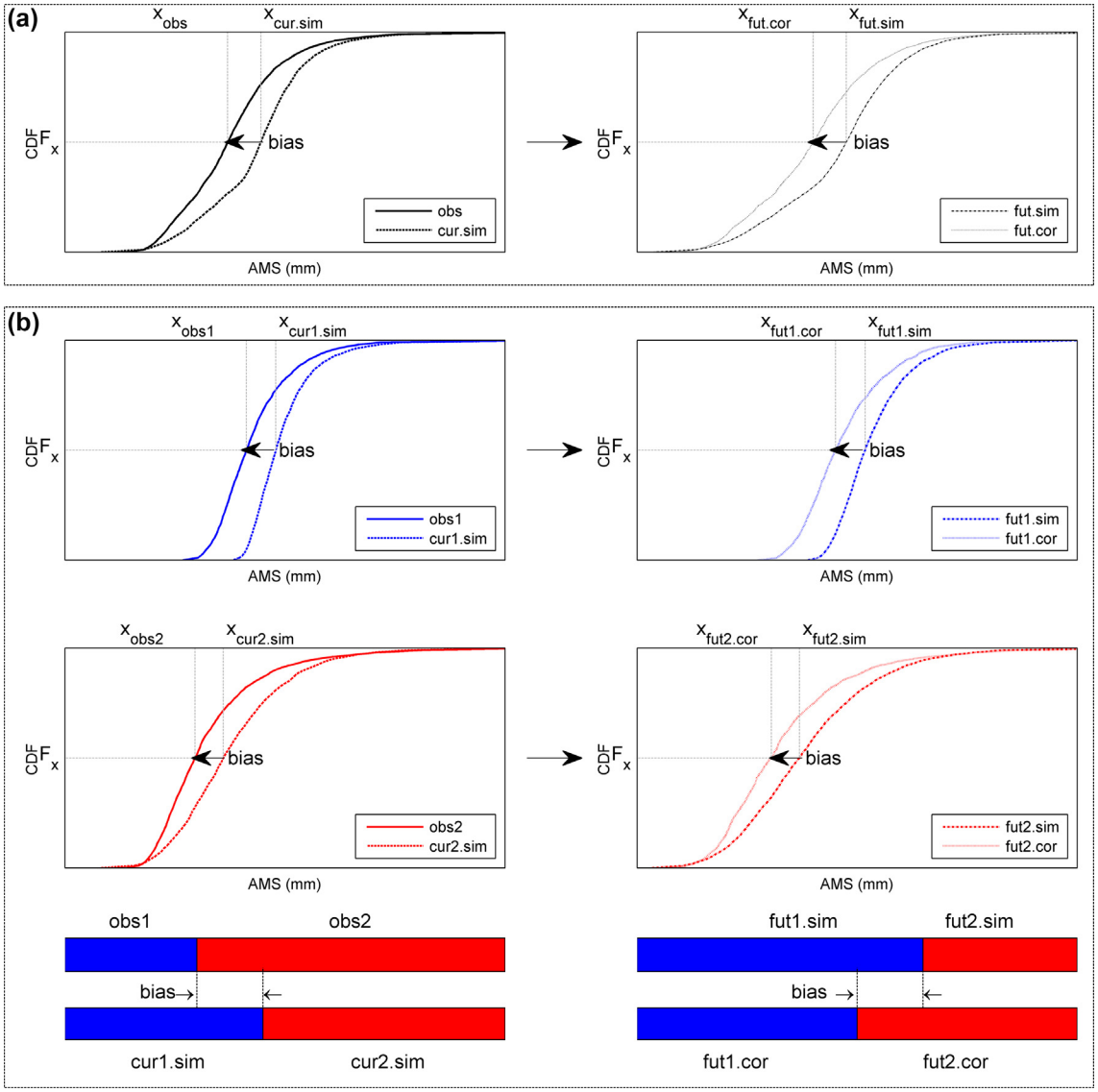

Fig. 2. Schematic description of the two different bias correction methods. (a) Quantile mapping; (b) synoptic pattern based bias correction. Different line styles represent different data source with solid line representing observations, dashed line current simulation, dash-dotted line future simulation, and dotted line future bias-corrected values. Colors indicate rainfall extremes associated with different synoptic patterns with blue indicating synoptic type 1, and red synoptic type 2. Black color on the panel (a) indicates the unclassified precipitation extremes. The bars at the bottom represent the weights of rainfall extremes for each synoptic type. (For interpretation of the references to color in this figure legend, the reader is referred to the web version of this article.)

3.1. Identifying extreme events

The 1-day extreme events were identified using 1-day annual maximum rainfall from observations. Since the synoptic-scale weather systems usually have diameters greater than 200 km (Kuo et al., 2015), it is unlikely that the rainfall extremes induced by synoptic-scale weather systems would occur at only a few individual stations. To avoid using synoptic classifications on days with only small local convective storms occurring, any days with at least one but less than five stations having concurrent annual maximum rainfall were pre-classified as small-scale event days. For days when at least five stations have concurrent annual maximum rainfall, we defined them as synoptic-scale event days, on which the synoptic classification was implemented. Based on these definitions, we found 313 small-scale events and 155 synoptic-scale events within the 20-year observational time period.

When considering the model domain, it is necessary to think about how to translate the above methodology to a gridded dataset rather than the relatively sparse gauge locations. As the station scale differs from the grid scale, a five-grid threshold would lead to many more events than 155. To find the appropriate size for the grid threshold to give the same number of extreme events as the station-based analysis, we used the RCM simulation driven by NNRP boundary conditions and varied the minimum number of grids with concurrent annual maxima. As the grid threshold increases, the number of large-scale extreme events in the domain decreases. We found that a 419-grid threshold led to exactly the same number of the synoptic-scale events as the observations. The 419-grid was also used as an upper threshold for identifying the lower threshold for the small-scale events (i.e. those occurring concurrently at one to four stations). The lower threshold for small-scale events was found to be 57 grid points, leading to 313 events in the RCM simulation driven by NNRP. These thresholds were also adopted to identify the extreme events from the RCM simulations driven by the CSIRO Mk3.5 GCM under both the current and future climates.

Table 2
The number of synoptic-scale and small-scale 1-day extreme events from observations and RCM simulations.

	No. of 1-day synoptic-scale events	No. of 1-day small-scale events
Observations	155	313
RCM/NNRP	155	313
RCM/Mk3.5 1990–2009	137	361
RCM/Mk3.5 2040–2059	147	465

Based on the identified grid thresholds, the number of synoptic-scale and small-scale extreme events and the days when these events occur were established for the GCM-driven RCM simulations under current and future climates. Table 2 shows the number of 1-day extreme events at the synoptic and small scales obtained from observations and model simulations. In general, the GCM-driven RCM simulated fewer synoptic-scale events and more small-scale events than observations under current climate conditions. This indicates that the GCM-driven RCM tends to overestimate the occurrence of the localized extreme events but misses some of the large spatial scale events. For the future climate, the number of extreme events simulated by the GCM-driven RCM at both synoptic and small scales increased from current climate simulations, which is consistent with other studies (Allan and Soden, 2008; O'Gorman, 2015; Wuebbles et al., 2013).

3.2. Synoptic climatological classification

The intensity and frequency of rainfall extremes are likely to vary with different synoptic weather patterns. In this study, a certain number of synoptic patterns were identified for the extreme event days using the self-organizing maps (SOM) classification. The SOM algorithm (Kohonen, 2001) provides an effective tool for visualizing the complex distribution of synoptic patterns by projecting the high-dimensional data onto a two-dimensional grid map. In atmospheric science, SOMs are commonly used to identify synoptic patterns (Argüeso et al., 2015; Hewitson and Crane, 2002; Schuenemann and Cassano, 2010).

The first step of the SOM classification is to define a random matrix of nodes within the input data sample space composed of the 155 synoptic maps identified in Section 3.1. Each node is a vector of the same length as each input data sample, which is 42 (i.e. 6×7 grid points) for the NNRP synoptic field and 925 (i.e. 25×37 grid points) for the RCM/NNRP synoptic filed. The second step is to assign each input data sample (i.e. 155 synoptic maps) to its closest node, according to the Euclidean distance. The third step is to select a node and identified one of all the assigned data samples over the neighborhood of the selected node such that the identified data sample has the smallest sum of distances from all the other data samples over this neighborhood. This identified data sample is called the generalized median and is used to replace the selected node. Step 4 is to repeat Step 3 for all other nodes. The above process from Step 2 to Step 4 is iterated until convergence, that is, the generalized median coincides with the selected node. Finally, all the days in each node are averaged, and the resultant mean represents one cluster. Therefore, the number of nodes is equal to the number of clusters.

Too many clusters will lead to the centroids of the neighboring clusters being indistinguishable, whereas too few clusters can cause loss of important details due to over-generalization of information (Yip et al., 2013). The optimal number of clusters is determined by the Calinski Harabasz index (*CHI*), which is defined as the ratio of between-cluster variance (VAR_B) to within-cluster variance (VAR_W) (Burn, 2014).

$$CHI = \frac{VAR_B}{VAR_W} \times \frac{N-K}{K-1} \quad (1)$$

$$VAR_B = \sum_{k=1}^{K} n_k \|z_k - z\|^2 \quad (2)$$

$$VAR_W = \sum_{k=1}^{K} \sum_{i=1}^{n_k} \|x_i - z_k\|^2 \quad (3)$$

Here, N is the number of observations. K is the number of clusters. z_k is the centroid of cluster k. z is the centroid of the entire data set. n_k is the number of observations (x_i) that belong to cluster k. In this study, CHI was calculated for K varying from 2 to 10 and the value of K for which CHI is maximized is considered to be the optimal number of clusters. Here a provisional 10 clusters were used as the maximum number of clusters. However, the estimated CHI in Section 4.2 shows a clear trend that CHI decreases with the number of clusters.

The synoptic patterns identified from the NNRP dataset were first compared with those obtained from the RCM/NNRP simulations regarding the number of clusters, the proportion of each cluster and the spatial presentation of each pattern. As the synoptic patterns identified from the RCM/NNRP simulations rather than the NNRP dataset were used as the base maps to extract the similar patterns from the RCM/MK3.5 under both current and future climates, an assumption made here is that the synoptic patterns simulated by RCM/NNRP are representative of observed ones. Therefore, it is desirable that the synoptic patterns of the RCM/NNRP be similar to those found for observations (i.e. NNRP). As the synoptic patterns are generally considered to be simulated well by RCMs, this assumption is sensible and was verified by comparing the synoptic patterns obtained from the two datasets (i.e. RCM/NNRP and NNRP) in Section 4.2. In finding the synoptic patterns for the RCM/MK3.5, the Euclidean distance between the base maps and the synoptic status on each of the days with synoptic-scale events simulated by the RCM/MK3.5 was estimated and the days with the synoptic status closest to one of the cluster base maps was assigned to that cluster.

3.3. Synoptic patterns based bias corrections

As the biases of the extreme rainfall vary with the different synoptic patterns; we adopted a synoptic pattern based bias correction method, which corrects not only the biases in the extreme rainfall corresponding to each synoptic type, but also the proportion of each type.

Fig. 2b illustrates the process of the SP-based bias correction method. To keep the presentation clear, we assume only two clusters are found in Section 3.2. Bias correction is applied to each individual cluster by means of quantile mapping, in which we first calculated the correction factors as the ratio of the observed rainfall extreme value to the model simulated value for the current climate for each percentile (X) for cluster k. The future model projection P_{mod}^{fut} is then corrected for each cluster at the percentile X by multiplying with the appropriate correction factor according to Eq. (4). The assumption made here is that biases in each type of extreme rainfall are constant over time. This assumption is different from the "constant bias" assumption often made in studies using GCM or RCM simulations (Gutjahr and Heinemann, 2013; Piani et al., 2010; Räty et al., 2014), which can be violated under a warmer climate as suggested by a few recent studies (Sunyer et al., 2014). In this study, the overall bias in the extreme rainfall distribution is not constant as we allow the proportion of each type of extreme rainfall event to change as well as the more standard assumption that the bias may be different for different parts of the rainfall distribution.

$$P_{cor}^{fut}(k,X) = \frac{P_{obs}(k,X)}{P_{\mathrm{mod}}^{cur}(k,X)} \times P_{\mathrm{mod}}^{fut}(k,X) \quad (4)$$

The weights simulated by the RCM are corrected for individual clusters following Eq. (5). The corrected future rainfall extremes for all the clusters are calculated as the weighted sum of the corrected rainfall extremes of all the individual clusters. The results are expected to be different from those obtained by applying quantile mapping bias correction to the entire dataset without classification as illustrated in Fig. 2a.

$$w_{cor}^{fut}(k) = w_{obs}(k) - w_{\mathrm{mod}}^{cur}(k) + w_{\mathrm{mod}}^{fut}(k) \quad (5)$$

$$P_{cor}^{fut}(X) = \sum_{k=1}^{K} w_{cor}^{fut}(k) P_{cor}^{fut}(k,X). \quad (6)$$

3.4. Synthetic experiment design

As there is only one high-resolution (2 km) RCM currently available over the study region, the concern is that any findings based on a single model may lack generality. To explore the possible conditions under which the proposed method will lead to significantly different outcomes, a synthetic experiment was designed. In the experiment, instead of using the annual maximum series (AMS) simulated by a single RCM, synthetic datasets that cover a wide range of possible AMS values were used. Each synthetic dataset was extracted from a Generalized Extreme Value (GEV) distribution. The GEV distribution was found to be the best fit for the AMS in Australia (Green et al., 2012). The GEV parameters used to build the synthetic AMS to represent the RCM simulations for both current and future climates were extracted from a sequence of GEV parameter sets, which were created by perturbing the observation GEV parameters to 50% above or below their actual values. To reduce the computation time, two AMS clusters corresponding to two different SPs were adopted in this experiment. The proportion of each cluster was selected from a sequence of the proportions that are within 50% above or below the observed proportion for that type. Repeating this data generating process for 2 million times and excluding the cases when the mean of the AMS is 50% above or below the observational mean and the proportion of each cluster is less than 2% or more than 98%, we ended up with 680,391 valid cases. We then applied the two bias correction methods to those valid cases and carried out a Kolmogorov–Smirnov (KS) test at 5% significance level on the results.

Based on the KS test results, the synthetic cases were split into two groups. One group shows the proposed method generates significantly different results to the quantile mapping method. The other group shows the results produced by the two methods are statistically indistinguishable. To investigate the possible conditions that can be used to predict the membership of these two groups, the classification tree method was used. The concept of the classification tree is to recursively split the data space of the predictors into two subsets until each subset contains the data with the response mainly belonging to a given class (Friedman et al., 2001). In this case, the two classes of the response were defined as the KS test decision (i.e. 0 for accepting the null hypothesis, and 1 for rejecting the null hypothesis) on whether the proposed method produces significantly different results to the conventional method. The following five factors considered to be able to potentially separate the significantly different cases from the insignificant ones were used as predictors of the classification tree.

- The absolute change in the proportion of each cluster, $\|w_{f1} - w_{c1}\|$, which can be any value between 0 and 1. Here, w_{c1} and w_{f1} represent the proportion of cluster 1 under the current and future climates, respectively. One important feature of the proposed method is that it considers the change in the proportion of each cluster, which is ignored by the quantile mapping approach. If there is no change in the proportion, then the proposed method will collapse to the quantile mapping method. If the change in the proportion is 1, which means one type of extreme events completely changes to another type, then the two methods will again produce the same results because there is essentially only one type of extreme rainfall events.
- The absolute difference of the correction factors between two clusters, $\int_{p=0}^{1} \|CF_1 - CF_2\| dp$, where p is the probability, and CF is the correction factor. The subscripts *1* and *2* represent the cluster 1 and cluster 2. If the correction factors for the two clusters are the same (i.e. $CF_1 = CF_2$), then the correction factor for the entire distribution will also be the same. In this case, it is not necessary to apply bias correction to individual clusters separately as it will not generate any results that are different from correcting the entire distribution at once. On the other hand, if this factor is large, it means that the correction applied to each type is more different, and thus larger differences are likely to show between the two methods.
- The absolute change in quantiles of the corrected AMS for each cluster, $\int_{p=0}^{1} \|X_{f1}^{cor} - X_{c1}^{cor}\| dp$ and $\int_{p=0}^{1} \|X_{f2}^{cor} - X_{c2}^{cor}\| dp$, where p is the probability, and X^{cor} represents the quantile. The subscripts f and c indicate the current and future climates, respectively. The numbers 1 and 2 in the subscripts represent cluster 1 and cluster 2. If there is no change in AMS from current to future, then the corrected distribution of AMS for the future climate will be the same as for the current climate, which has to match observations. In this case, unless there is a dramatic change in the proportion of each cluster, the results obtained from the proposed method will be of no difference to those produced by using the quantile mapping method.
- The KS test decision (i.e. 0 for accepting the null hypothesis, and 1 for rejecting the null hypothesis) on whether the corrected distributions of the two clusters for the future climate are significantly different from each other, $H(X_{f1}^{cor}, X_{f2}^{cor})$. Here, X_{f1}^{cor} and X_{f2}^{cor} represent the quantiles of the corrected future AMS distributions for cluster 1 and cluster 2, respectively. The null hypothesis is that the two distributions are the same. A reject of the null hypothesis means that the corrected distributions of the two clusters for the future climate are different at 5% significance level, in which case the difference between the two methods are likely to show.

4. Results

As the synthetic experiment explores a wide range of possible extreme rainfall data spectrum, the results of it will be more general than the case study based on a single RCM. It is intuitive to report the general results first, and then go to the specific case. Therefore, this section will first inspect the outcomes from applying the two bias correction methods to the synthetic data, followed by a real case study based on RCM simulations. The results of the real case will be present in two subsections. First, the synoptic patterns identified using the SOM classification will be explained, and then the bias corrected future extreme rainfall distributions using the two methods will be compared.

4.1. Bias correction of synthetic data

The two bias correction methods were applied to the 680,391 synthetic cases, and the KS-test was used to test the difference

between the outcomes of the two methods. The result reveals that about 46% of the cases show the two bias corrected distributions under the future climate are significantly different from each other. This result provides insights into the likelihood of the two methods showing significant difference if multiple RCMs were available and used in this study, which is possible in the future due to the increasingly improved computer power.

To investigate the possible conditions under which the proposed method will significantly differ from the quantile mapping method, the classification tree approach was employed to separate the synthetic cases into the two distinctive groups. As explained in the previous section, the classification tree will recursively split the data into two subsets until each subset contains the data with the response mainly from the same class. It is necessary to know when to stop growing the tree. This is because an undergrown tree may cause some important structural information about the sample space missing, whereas an overgrown tree can result in overfitting of the training data. The optimal size of the tree is determined based on the minimum cross-validation error. It was found that cross-validation error decreases rapidly with the minimum leaf size, which is the minimum data points on any end node of the tree, and then slowly increases. The minimum leaf size found in this case is 359 with the cross-validation error of 0.2038. The optimal tree was grown based on this minimum leaf size.

Although the optimal tree has the lowest cross-validation error, the size is too big (i.e. 81 levels) to have any practical meaning, as it is unrealistic to apply 81 rules to get a decision on whether the two methods give different results. In fact, to get good separation of the significant cases from the insignificant ones, it is unnecessary to apply all the 81 rules. Only applying the rule at the first level from the root node is able to get 71% significant cases and 81% insignificant cases correctly classified as shown in Fig. 3. The averaged distributions for the future climate using the two methods were plotted for the cases that fall into the two branches of the tree at the first level. It is clear that cases on the left branch show the high similarity between the two methods while those on the right branch allow the proposed method to distinguish from the conventional method. The factor used in the classification at this level of

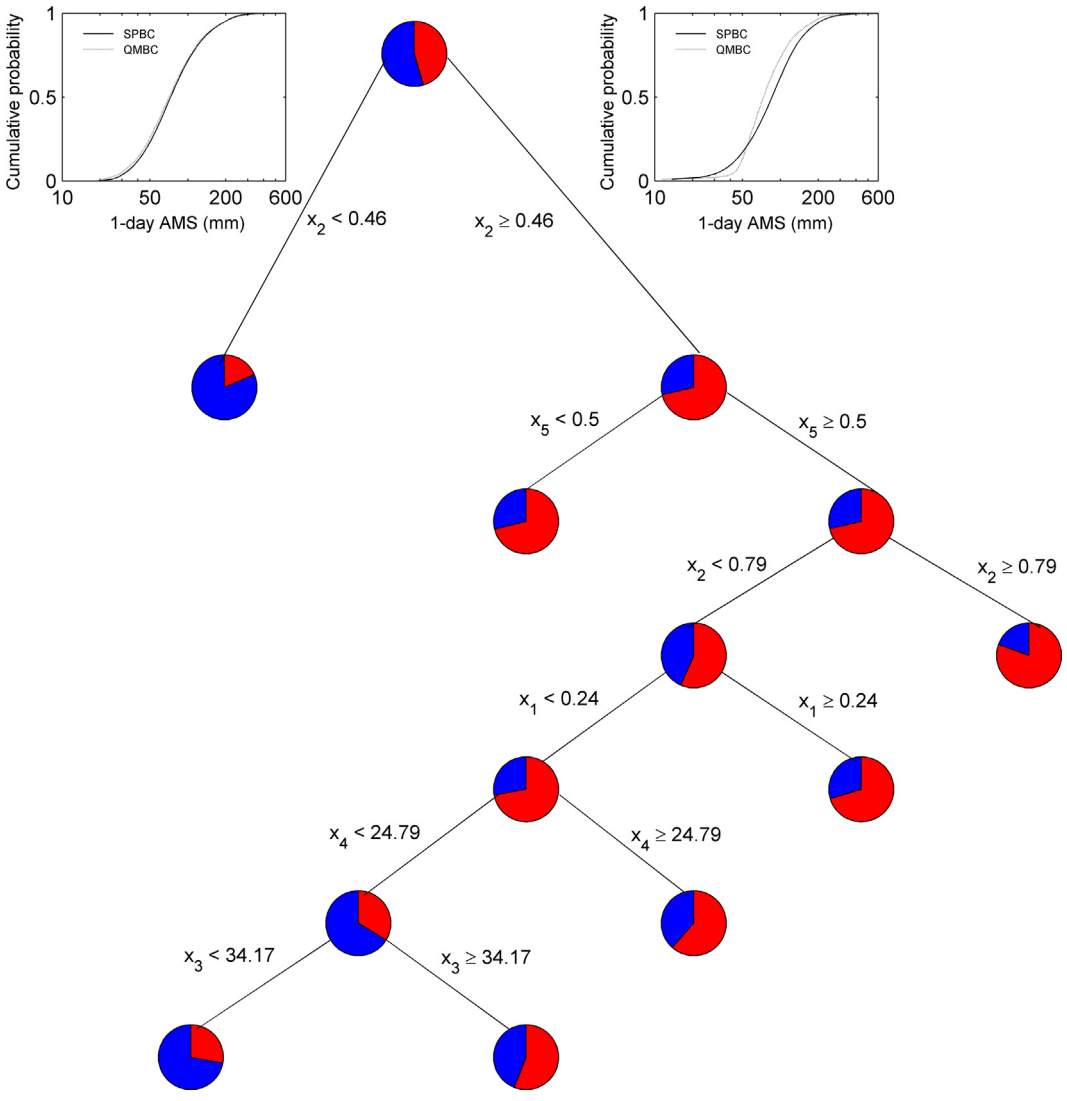

Fig. 3. Classification tree used to separate significant different results (red) from insignificant ones (blue). The tree is pruned to focus on the important details. x_i is the criteria used to splitting data at each node. x_1 is the absolute change in the proportion of each cluster; x_2 is the absolute difference of the correction factors between two clusters, x_3 and x_4 are the absolute change in quantiles of the corrected AMS for cluster 1 and cluster 2, respectively; and x_5 is the KS test decision (i.e. 0 for accepting the null hypothesis, and 1 for rejecting the null hypothesis) on whether the corrected distributions of the two clusters for the future climate are significantly different from each other. The bias corrected distributions using the two methods are plotted for the cases falling into the left (right) branch of the first level of the tree. (For interpretation of the references to color in this figure legend, the reader is referred to the web version of this article.)

the tree is the absolute difference of the correction factors between two clusters. When this factor is larger than 0.46, the two methods are most likely to generate significantly different results. This rule can be used as an initial checkpoint to see whether a different result is expected when bias correction is required for a new dataset. It is noted from Fig. 3 that as the tree grows down, the misclassification rate does not necessarily drop, which suggests that the best segregation line draws at the first level of the tree. This means that the absolute difference of the correction factors between two clusters is the dominant factor that contributes to the difference between the two methods.

4.2. Synoptic patterns of observations and model simulations

Despite the factor that nearly half of the synthetic cases proved that applying bias correction to partitioned extreme rainfall data does generate significantly different results compared to when the types of rainfall extremes are ignored, it is still worthwhile to test the findings through a case study using actual RCM simulations.

The sea level pressure from NNRP dataset during the extreme events were classified into various numbers of clusters starting from 2 to 10. According to the Calinski Harabasz index, two clusters are favored for 1-day extreme events. Taking the small-scale extreme events as a third cluster, a total of three clusters can be used to represent all the extreme rainfall events identified (Table 2). By taking the average of the synoptic maps that belong to their corresponding classes, the representative synoptic patterns (SPs) were obtained. Fig. 4a–c shows the representative SPs for the three clusters, all of which have a high over the Tasman Sea and a low over the continent. The moisture transported from the sea to the land by the pressure gradient brought heavy rainfall to the Sydney region. It is noted that SP3 has the sparsest contours, which is expected since this cluster is identified for days with only 1–4 stations having concurrent annual maximum rainfall. SP2 has the densest contours, indicating the cluster represents the extreme events with strongest winds.

As the pressure field from the RCM used in this study is on a finer grid resolution than that from the NNRP dataset, the synoptic patterns identified from the NNRP dataset cannot be used as base maps to establish the synoptic clusters for the RCM runs. Instead, the synoptic patterns found from the RCM/NNRP simulations by applying the SOM classification was used as the base maps, which are shown in Fig. 4d–f. The legitimacy of using RCM/NNRP simulated synoptic patterns as observation is confirmed by the fact that the synoptic patterns simulated by the RCM/NNRP are similar to those found from observations (i.e. NNRP) despite the different resolutions of the pressure field from these two data sources.

The synoptic maps on each of the extreme event days defined by the RCM/MK3.5 simulations for the current climate were assigned to the closest base map according to the Euclidean distance. Fig. 4g–i is the three representative synoptic patterns after taking the average of all the synoptic maps that belong to each cluster. Although these three synoptic clusters are similar to those found from the RCM/NNRP simulations, the proportion of each cluster differs from that of the RCM/NNRP run. The RCM/MK3.5 tends to undersimulate the occurrence of the synoptic-scale events (i.e. SP1 and SP2), while overproduces the number of the small-scale events (i.e. SP3). This proportional discrepancy is considered as one type of bias (i.e. bias in the proportion) and needs to be corrected.

Again, based on the Euclidean distance the three clusters were identified for the RCM/MK3.5 for the future climate as shown in Fig. 4j–l. These three patterns are also similar to those simulated by the RCM/NNRP. Here a clear decreasing trend is seen in the proportion of the synoptic-scale events (i.e. SP1 and SP2), whereas an increasing trend is found in the proportion of the small-scale events (i.e. SP3). Although the proportion of the synoptic-scale events is decreasing, the occurrence or the number of this type of events is still increasing but not as fast as the small-scale events as indicated in Table 2.

4.3. Bias correction of the RCM simulations

Based on the classification results, the annual maximum rainfall time series belonging to the same cluster were grouped together. The distribution of each cluster was bias corrected using Eq. (4). The proportion of each cluster was also corrected and then multiplied to the corrected distribution of that cluster. Finally, the weighted distributions of the three clusters were added up to form the whole distribution, which was compared with the distribution obtained using the quantile mapping bias correction method. It is clear that extreme rainfall intensity tends to increase for events with exceedance probability smaller than 1 in 5 years (i.e. less frequent events) as indicated by comparing the 1-day AMS between observations and the future simulation after bias correction (Fig. 5e). This increasing trend was also found in the individual type of precipitation extremes corresponding to SP1 and SP3 as indicated by the blue and green curves in Fig. 5a and b, with SP1-related precipitation extremes increasing the most. The intensity of the precipitation extremes belonging to SP2 was to change little in the future. For this particular RCM, the empirical CDF obtained from the proposed method differs from that estimated from the conventional quantile mapping method by −10% to 8% as shown in Fig. 5f, although the KS test does not indicate this difference is statistically significant at the 5% level. The between-cluster difference in the correction factor estimated for this RCM simulation is 0.18, which falls into the first left branch of the classification tree. This confirms the non-significant results from the KS test.

5. Discussions

When designing the synthetic experiment, we used only two clusters for the simplicity of demonstration. The classification tree can give us a sense of when we can expect different results from the two methods. Although the situation may become much more complicated with an increasing number of clusters, we can still expect a higher likelihood of finding differences between the two methods if large differences are identified in correction factors between different extreme rainfall types. Alternatively, we can also draw a classification tree to find the rules to distinguish significant cases from insignificant ones, but this time the tree is based on more factors. For example, when only two clusters are used, the absolute difference in the correction factor is just between cluster 1 and 2. When a third cluster is added, the difference between cluster 1 and 3, as well as between cluster 2 and 3 should also be included.

The RCM used in this study adopted CMIP3 GCM (CSIRO MK3.5) outputs as its boundary conditions for the future run because the CMIP5 project was in its early stage when the RCM project (NARCliM) was initiated in 2011. The future RCM projection used the SRES A2 emission scenario, which has the same greenhouse emission as Representative Concentration Pathway (RCP) 6.0 and RCP 4.5 in 2050. As suggested by Woldemeskel et al. (2016), the uncertainty in temperature simulated by CMIP5 GCMs is of the same order as that simulated by CMIP3 CCMs, while a slight reduction in precipitation uncertainty is found due to the improvement of model structure and realization in CMIP5. Therefore, using a CMIP3 GCM for boundary conditions is unlikely to change the conclusion in this study compared to using a CMIP5 GCM.

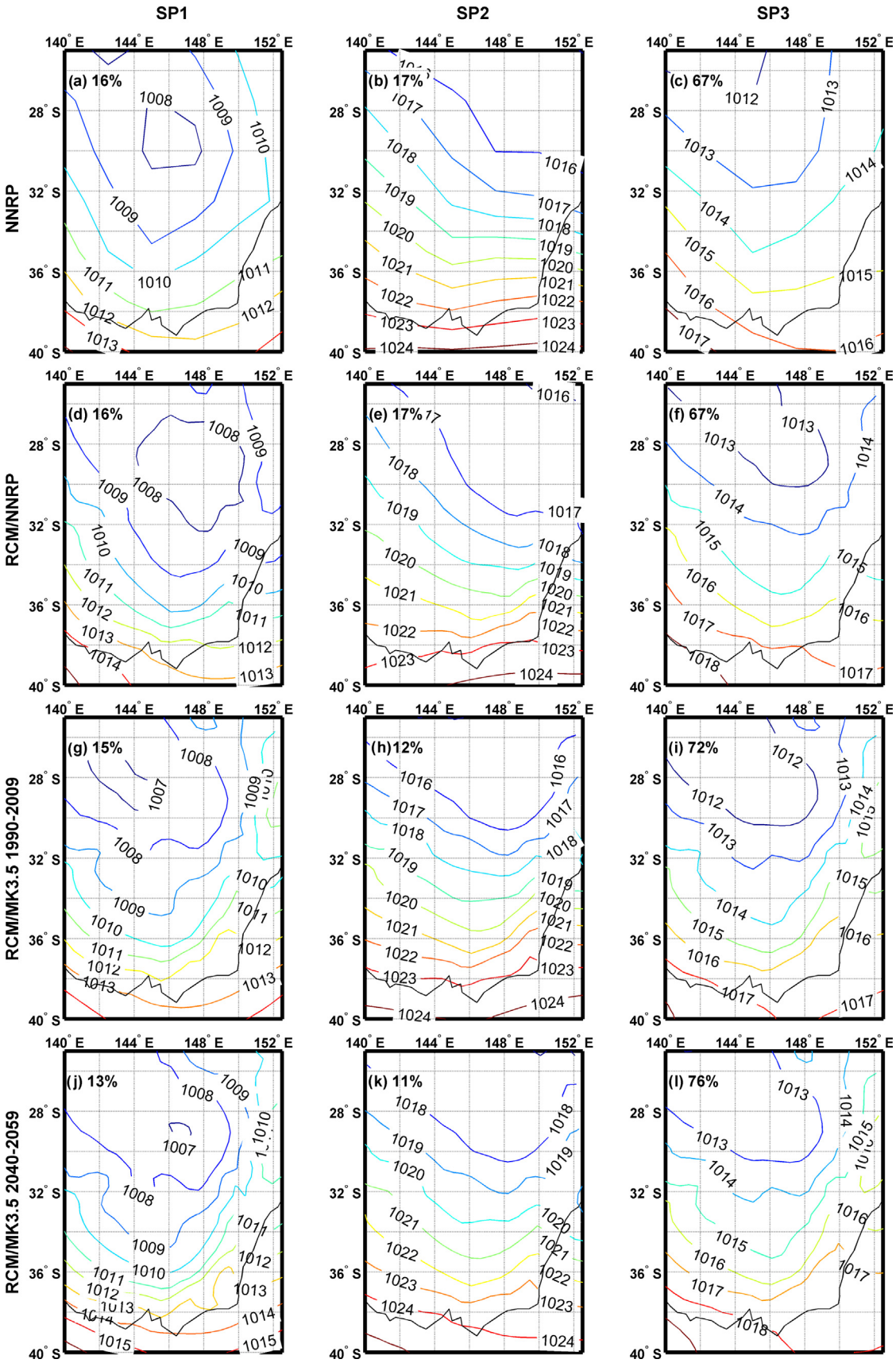

Fig. 4. The 1-day synoptic weather patterns captured by NNRP, RCM/NNRP, RCM/MK3.5 1990–2009 and RCM/MK3.5 2040–2059.

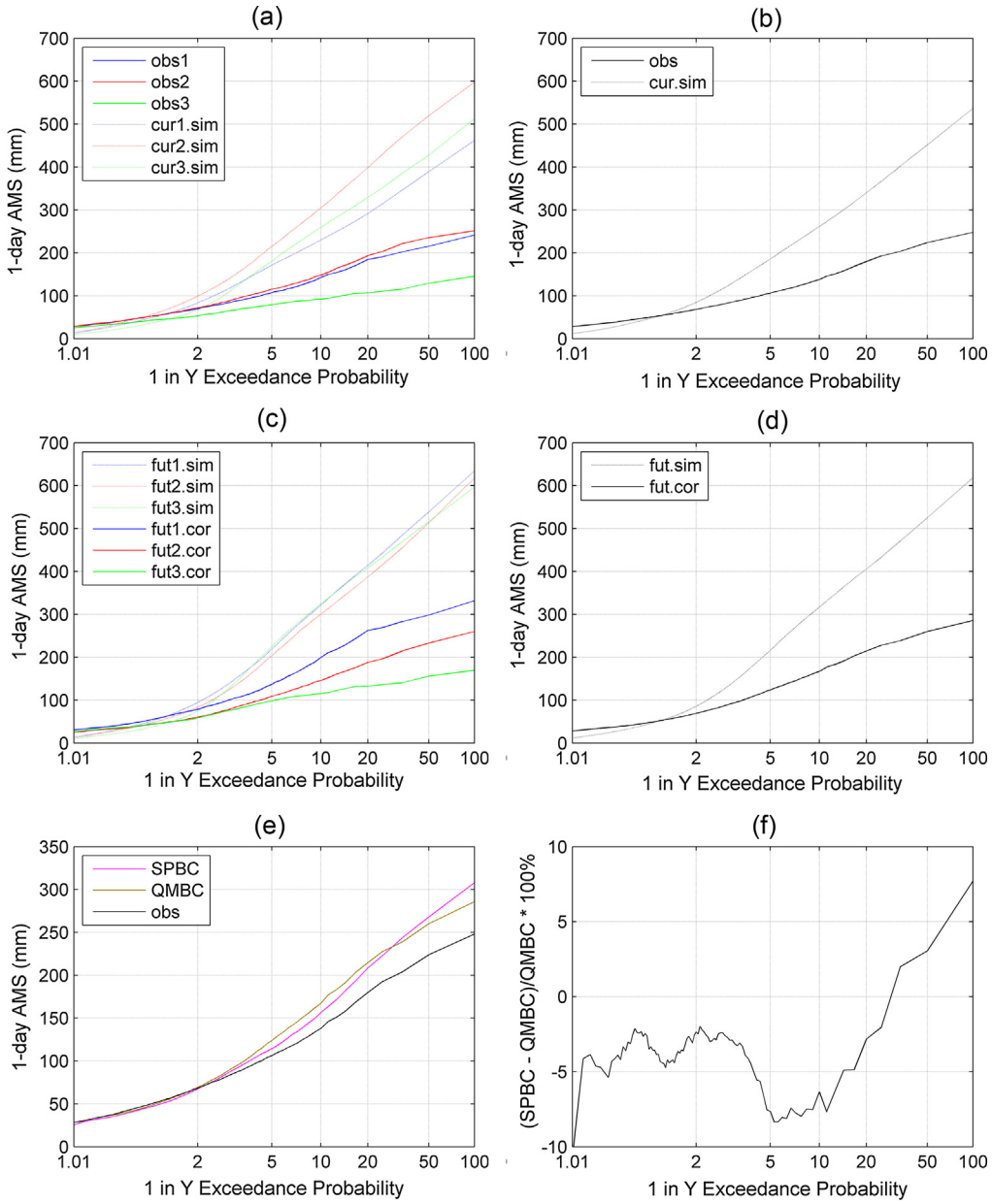

Fig. 5. 1-day AMS for various exceedance probabilities for (a) the three different clusters from the observations and current model simulations; (b) the overall data from the observations and current model simulations; (c) the three different clusters from the future model simulations with and without bias correction; (d) the overall data from future model simulations with and without bias correction; (e) future model simulations after adopting synoptic pattern based bias correction (SPBC) and quantile mapping bias correction (QMBC) compared with current observations; (f) the relative difference (%) in the corrected 1-day AMS using the two bias correction methods.

The results presented here for the case study are only for 1-day AMS. We have also applied the SOM classification to the 3-day mean sea level pressure and then carried out the SP-based bias correction method on 3-day AMS. The results were compared with those based on the quantile mapping. Similar to 1-day case, a non-significant difference was found between the corrected future extreme rainfall distributions obtained from the two methods. For the 3-day case, the between-cluster difference in the correction factor was found to be 0.19, also falling into the first left branch of the classification tree. This again confirms the finding that the difference between the two methods is not significant for this particular RCM run.

Unlike most other bias correction approaches, which are based on a crucial assumption that the bias is stationary, the proposed method allows a non-stationary bias in the overall distribution of extreme rainfall by incorporating the possible changes in the mix of different types of extreme rainfall. However, the proposed method assumes that there is no change in the bias of each type of extreme rainfall event. This assumption is difficult to verify because the historical period simulated by the RCM used in this study is not long enough to show any non-stationary trend in bias. We note that recent studies that question the stationarity assumption only refer to bias of the overall distribution of the climate variables. There is no research, to our knowledge, that examines the non-stationarity in the bias of different types of events.

This study applied the SP-based bias correction method only to daily and 3-day AMS in the Sydney region. Although we did find significantly different results obtained from the SP-based method

and the conventional method in nearly half (47%) of the synthetic cases, the single RCM simulation cannot distinguish these two methods. The reason for that is the difference in the correction factors between different types of rainfall extremes is not large enough to make the results statistically distinguishable.

In addition to using sea level pressure only to represent the synoptic patterns that are responsible for the extreme rainfall event, multiple variables (including the precipitable water, vertical velocity at 850 hPa and relative vorticity at 500 hPa) were also used to partition the extreme rainfall events into various types. The selection of these variables was based on a previous study by Friederichs and Hense (2007), which used these variables to statistically downscale extreme rainfall over Europe. However, using multivariables to define SPs caused only a small change in the results. The conclusion is still the same that the influence of the additional information of SPs on the bias correction is not significant for this particular RCM.

Now the question remains whether a different conclusion can be reached if the same process was applied to subdaily AMS and to other parts of the world. Unlike daily or multiday rainfall extremes, subdaily extremes are more related to convective storms than stratiform systems. The response of convective rainfall to temperature increases is different to that of stratiform rainfall. In general, convective events are more sensitive to temperature changes than stratiform storms and changes in the intensity of extreme events may be related to a change in the proportion of convective versus stratiform events (Berg and Haerter, 2013). Westra et al. (2014) did a thorough review on future changes of subdaily extreme rainfall and pointed out the limitation in the current state of knowledge on this issue. However, it is clear that the trend of subdaily extreme rainfall varies with temperature, regions and storm durations, etc. Therefore, it is possible to see significantly different bias correction results from these two methods when they are applied to a different region and different time scale to our case study here.

6. Conclusions

Potential changes in synoptic circulation patterns under global warming are expected to alter the intensities and frequencies of rainfall extremes. In this study, we evaluated the influence of including synoptic patterns to the bias correction first through a synthetic experiment and then a real case based on RCM simulations. We found 46% of the synthetic cases turned out to be significantly different when using the two bias correction methods. For the results to be significantly different, the between-cluster difference in the correction factor needs to be large enough, which, however, is not the case for the RCM simulations used in this study.

To identify the different extreme rainfall clusters, the self-organizing maps classification was used. The three SPs identified for the NNRP reanalysis dataset closely resemble those simulated by WRF/NNRP, which confirms the initial assumption that the circulation patterns are generally simulated well by the RCMs. Using the identified SPs from the WRF/NNRP simulation as base maps, the synoptic maps on the extreme rainfall days simulated by WRF/MK3.5 for both the current and future climates were allocated to the closest base map according to the Euclidean distance. It was found that the total number of extreme events tends to increase under a warming climate and that the number of small-scale extreme events increases faster than that of large-scale extreme events. This finding is consistent with the previous study that localized convective storms are more sensitive to higher temperature (Berg et al., 2013).

Acknowledgements

Regional climate data have been provided by the New South Wales and Australian Capital Territory Regional Climate Model (NARCliM) project funded by NSW Governmental Office of Environment and Heritage, University of New South Wales Climate Change Research Centre (CCRC), ACT Government Environment and Sustainable Development Directorate and other project partners. This work was made possible by funding from the NSW Environment Trust (RM08603), as well as the Australian Research Council (DP120100338 and FT110100576). This work was supported by an award under the Merit Allocation Scheme on the NCI National Facility at the ANU.

References

Alexander, L.V. et al., 2006. Global observed changes in daily climate extremes of temperature and precipitation. J. Geophys. Res.: Atmos. 111 (D5), D05109. http://dx.doi.org/10.1029/2005JD006290.

Allan, R.P., Soden, B.J., 2008. Atmospheric warming and the amplification of precipitation extremes. Science 321 (5895), 1481–1484. http://dx.doi.org/10.1126/science.1160787.

Argüeso, D., Evans, J.P., Fita, L., 2013. Precipitation bias correction of very high resolution regional climate models. Hydrol. Earth Syst. Sci. Discuss. 10 (6), 8145–8165. http://dx.doi.org/10.5194/hessd-10-8145-2013.

Argüeso, D., Evans, J.P., Fita, L., Bormann, K.J., 2014. Temperature response to future urbanization and climate change. Clim. Dyn. 42 (7), 2183–2199. http://dx.doi.org/10.1007/s00382-013-1789-6.

Argüeso, D., Evans, J.P., Pitman, A.J., Di Luca, A., 2015. Effects of city expansion on heat stress under climate change conditions. PLoS One 10 (2), e0117066.

Bárdossy, A., Pegram, G., 2011. Downscaling precipitation using regional climate models and circulation patterns toward hydrology. Water Resour. Res. 47 (4), W04505. http://dx.doi.org/10.1029/2010WR009689.

Berg, P., Haerter, J.O., 2013. Unexpected increase in precipitation intensity with temperature – a result of mixing of precipitation types? Atmos. Res. 119, 56–61. http://dx.doi.org/10.1016/j.atmosres.2011.05.012.

Berg, P., Moseley, C., Haerter, J.O., 2013. Strong increase in convective precipitation in response to higher temperatures. Nat. Geosci. 6 (3), 181–185, doi: http://www.nature.com/ngeo/journal/v6/n3/abs/ngeo1731.html#supplementary-information.

Bordoy, R., Burlando, P., 2012. Bias correction of regional climate model simulations in a region of complex orography. J. Appl. Meteorol. Climatol. 52 (1), 82–101. http://dx.doi.org/10.1175/JAMC-D-11-0149.1.

BoroumandJazi, G., Saidur, R., Rismanchi, B., Mekhilef, S., 2012. A review on the relation between the energy and exergy efficiency analysis and the technical characteristic of the renewable energy systems. Renew. Sustain. Energy Rev. 16 (5), 3131–3135. http://dx.doi.org/10.1016/j.rser.2012.02.057.

Burn, D.H., 2014. A framework for regional estimation of intensity-duration-frequency (IDF) curves. Hydrol. Process. 28 (14), 4209–4218. http://dx.doi.org/10.1002/hyp.10231.

Carton, J.A., Giese, B.S., 2008. A reanalysis of ocean climate using simple ocean data assimilation (SODA). Mon. Weather Rev. 136 (8), 2999–3017. http://dx.doi.org/10.1175/2007MWR1978.1.

Chandra, R., Saha, U., Mujumdar, P.P., 2015. Model and parameter uncertainty in IDF relationships under climate change. Adv. Water Resour. 79, 127–139. http://dx.doi.org/10.1016/j.advwatres.2015.02.011.

Clemons, T.E., Bradley Jr., E.L., 2000. A nonparametric measure of the overlapping coefficient. Comput. Stat. Data Anal. 34 (1), 51–61. http://dx.doi.org/10.1016/S0167-9473(99)00074-2.

Evans, J.P., McCabe, M.F., 2010. Regional climate simulation over Australia's Murray–Darling basin: a multitemporal assessment. J. Geophys. Res.: Atmos. 115 (D14). http://dx.doi.org/10.1029/2010JD013816, n/a–n/a.

Evans, J.P., McCabe, M.F., 2013. Effect of model resolution on a regional climate model simulation over southeast Australia. Clim. Res. 56 (2), 131–145. http://dx.doi.org/10.3354/cr01151.

Evans, J.P., Westra, S., 2012. Investigating the mechanisms of diurnal rainfall variability using a regional climate model. J. Clim. 25 (20), 7232–7247. http://dx.doi.org/10.1175/JCLI-D-11-00616.1.

Frei, C., Schöll, R., Fukutome, S., Schmidli, J., Vidale, P.L., 2006. Future change of precipitation extremes in Europe: intercomparison of scenarios from regional climate models. J. Geophys. Res.: Atmos. (1984–2012) 111 (D6).

Friederichs, P., 2010. Statistical downscaling of extreme precipitation events using extreme value theory. Extremes 13 (2), 109–132. http://dx.doi.org/10.1007/s10687-010-0107-5.

Friederichs, P., Hense, A., 2007. Statistical downscaling of extreme precipitation events using censored quantile regression. Mon. Weather Rev. 135 (6), 2365–2378. http://dx.doi.org/10.1175/MWR3403.1.

Friedman, J., Hastie, T., Tibshirani, R., 2001. The elements of statistical learning, 1. Springer Series in Statistics. Springer, Berlin.

Green, J., Xuereb, K., Johnson, F., Moore, G., The, C., 2012. The revised intensity-frequency-duration (IFD) design rainfall estimates for Australia – an overview.

In: 34th Hydrology and Water Resources Symposium 2012, Engineers Australia, Sydney, pp. 808–815.
Grillakis, M.G., Koutroulis, A.G., Tsanis, I.K., 2013. Multisegment statistical bias correction of daily GCM precipitation output. J. Geophys. Res.: Atmos. 118 (8), 3150–3162. http://dx.doi.org/10.1002/jgrd.50323.
Gudmundsson, L., Bremnes, J.B., Haugen, J.E., Engen-Skaugen, T., 2012. Technical note: downscaling RCM precipitation to the station scale using statistical transformations – a comparison of methods. Hydrol. Earth Syst. Sci. 16 (9), 3383–3390. http://dx.doi.org/10.5194/hess-16-3383-2012.
Gutjahr, O., Heinemann, G., 2013. Comparing precipitation bias correction methods for high-resolution regional climate simulations using COSMO-CLM. Theor. Appl. Climatol. 114 (3–4), 511–529. http://dx.doi.org/10.1007/s00704-013-0834-z.
Hewitson, B.C., Crane, R.G., 2002. Self-organizing maps: applications to synoptic climatology. Clim. Res. 22 (1), 13–26. http://dx.doi.org/10.3354/cr022013.
Horton, D.E. et al., 2015. Contribution of changes in atmospheric circulation patterns to extreme temperature trends. Nature 522 (7557), 465–469. http://dx.doi.org/10.1038/nature14550.
Ishak, E., Rahman, A., Westra, S., Sharma, A., Kuczera, G., 2013. Evaluating the non-stationarity of Australian annual maximum flood. J. Hydrol. 494, 134–145.
Johnson, F., Sharma, A., 2012. A nesting model for bias correction of variability at multiple time scales in general circulation model precipitation simulations. Water Resour. Res. 48 (1), W01504. http://dx.doi.org/10.1029/2011WR010464.
Kohonen, T., 2001. Self-organizing maps. Ser. Information Sciences, vol. 30. Springer, Berlin.
Kuo, C.C., Gan, T.Y., Gizaw, M., 2015. Potential impact of climate change on intensity duration frequency curves of central Alberta. Climatic Change. http://dx.doi.org/10.1007/s10584-015-1347-9.
Lafon, T., Dadson, S., Buys, G., Prudhomme, C., 2013. Bias correction of daily precipitation simulated by a regional climate model: a comparison of methods. Int. J. Climatol. 33 (6), 1367–1381. http://dx.doi.org/10.1002/joc.3518.
Li, J., Sharma, A., Johnson, F., Evans, J., 2015. Evaluating the effect of climate change on areal reduction factors using regional climate model projections. J. Hydrol. 528, 419–434. http://dx.doi.org/10.1016/j.jhydrol.2015.06.067.
Nguyen, H., Mehrotra, R., Sharma, A., 2016. Correcting for systematic biases in GCM simulations in the frequency domain. J. Hydrol. 538, 117–126. http://dx.doi.org/10.1016/j.jhydrol.2016.04.018.
O'Gorman, P., 2015. Precipitation extremes under climate change. Curr. Clim. Change Rep. 1 (2), 49–59. http://dx.doi.org/10.1007/s40641-015-0009-3.
Olsson, J., Berg, P., Kawamura, A., 2014. Impact of RCM spatial resolution on the reproduction of local, subdaily precipitation. J. Hydrometeorol. 16 (2), 534–547. http://dx.doi.org/10.1175/JHM-D-14-0007.1.
Piani, C., Haerter, J.O., Coppola, E., 2010. Statistical bias correction for daily precipitation in regional climate models over Europe. Theor. Appl. Climatol. 99 (1–2), 187–192. http://dx.doi.org/10.1007/s00704-009-0134-9.
Raneesh, K., Thampi, S., 2013. Bias correction for RCM predictions of precipitation and temperature in the Chaliyar River basin. J. Climatol. Weather Forecast.
Räty, O., Räisänen, J., Ylhäisi, J., 2014. Evaluation of delta change and bias correction methods for future daily precipitation: intermodel cross-validation using ENSEMBLES simulations. Clim. Dyn. 42 (9–10), 2287–2303. http://dx.doi.org/10.1007/s00382-014-2130-8.
Sachindra, D.A., Huang, F., Barton, A., Perera, B.J.C., 2014. Statistical downscaling of general circulation model outputs to precipitation—Part 2: Bias-correction and future projections. Int. J. Climatol. 34 (11), 3282–3303. http://dx.doi.org/10.1002/joc.3915.
Schuenemann, K.C., Cassano, J.J., 2010. Changes in synoptic weather patterns and Greenland precipitation in the 20th and 21st centuries: 2. Analysis of 21st century atmospheric changes using self-organizing maps. J. Geophys. Res.: Atmos. 115 (D5), D05108. http://dx.doi.org/10.1029/2009JD011706.
Singleton, A., Toumi, R., 2013. Super-Clausius–Clapeyron scaling of rainfall in a model squall line. Quart. J. Roy. Meteorol. Soc. 139 (671), 334–339. http://dx.doi.org/10.1002/qj.1919.
Sunyer, M.A. et al., 2015. Inter-comparison of statistical downscaling methods for projection of extreme precipitation in Europe. Hydrol. Earth Syst. Sci. 19 (4), 1827–1847. http://dx.doi.org/10.5194/hess-19-1827-2015.
Sunyer, M.A., Madsen, H., Rosbjerg, D., Arnbjerg-Nielsen, K., 2014. A Bayesian approach for uncertainty quantification of extreme precipitation projections including climate model interdependency and nonstationary bias. J. Clim. 27 (18), 7113–7132.
Thompson, G., Rasmussen, R.M., Manning, K., 2004. Explicit forecasts of winter precipitation using an improved bulk microphysics scheme. Part I: description and sensitivity analysis. Mon. Weather Rev. 132 (2), 519–542. http://dx.doi.org/10.1175/1520-0493(2004)132<0519:EFOWPU>2.0.CO;2.
Wasko, C., Sharma, A., 2015. Steeper temporal distribution of rain intensity at higher temperatures within Australian storms. Nat. Geosci. http://dx.doi.org/10.1038/ngeo2456, advance online publication.
Westra, S. et al., 2014. Future changes to the intensity and frequency of short-duration extreme rainfall. Rev. Geophys. 52 (3), 522–555. http://dx.doi.org/10.1002/2014RG000464.
Woldemeskel, F.M., Sharma, A., Sivakumar, B., Mehrotra, R., 2016. Quantification of precipitation and temperature uncertainties simulated by CMIP3 and CMIP5 models. J. Geophys. Res.: Atmos. 121 (1), 3–17. http://dx.doi.org/10.1002/2015JD023719.
Wong, G. et al., 2014. Stochastic model output statistics for bias correcting and downscaling precipitation including extremes. J. Clim. 27 (18), 6940–6959. http://dx.doi.org/10.1175/JCLI-D-13-00604.1.
Wuebbles, D. et al., 2013. CMIP5 climate model analyses: climate extremes in the United States. Bull. Am. Meteorol. Soc. 95 (4), 571–583. http://dx.doi.org/10.1175/BAMS-D-12-00172.1.
Yip, K.Y., Cheng, C., Gerstein, M., 2013. Machine learning and genome annotation: a match meant to be? Genome Biol. 14 (5), 205. http://dx.doi.org/10.1186/gb-2013-14-5-205.